# Structures of the four subfamilies of phosphodiesterase-4 provide insight into the selectivity of their inhibitors

Huanchen WANG*, Ming-Sheng PENG†, Yi CHEN†, Jie GENG*, Howard ROBINSON‡, Miles D. HOUSLAY§, Jiwen CAI†[1] and Hengming KE*[1]

*Department of Biochemistry and Biophysics and Lineberger Comprehensive Cancer Center, University of North Carolina, Chapel Hill, NC 27599–7260, U.S.A., †School of Chemistry and Chemical Engineering, and Structural Biology Laboratory, School of Pharmaceutical Sciences, Sun Yat-Sen University, Guangzhou, 510275, China, ‡Biology Department, Brookhaven National Laboratory, Upton, NY 11973–5000, U.S.A., and §Molecular Pharmacology Group, Wolfson Link Building, Division of Biochemistry and Molecular Biology, Institute of Biomedical and Life Sciences, University of Glasgow, Glasgow G12 8QQ, Scotland, U.K.

PDE4 (phosphodiesterase-4)-selective inhibitors have attracted much attention as potential therapeutics for the treatment of both depression and major inflammatory diseases, but their practical application has been compromised by side effects. A possible cause for the side effects is that current PDE4-selective inhibitors similarly inhibit isoforms from all four PDE4 subfamilies. The development of PDE4 subfamily-selective inhibitors has been hampered by a lack of structural information. In the present study, we rectify this by providing the crystal structures of the catalytic domains of PDE4A, PDE4B and PDE4D in complex with the PDE4 inhibitor NVP {4-[8-(3-nitrophenyl)-[1,7]naphthyridin-6-yl]benzoic acid} as well as the unliganded PDE4C structure. NVP binds in the same conformation to the deep cAMP substrate pocket and interacts with the same residues in each instance. However, detailed structural comparison reveals significant conformational differences. Although the active sites of PDE4B and PDE4D are mostly comparable, PDE4A shows significant displacements of the residues next to the invariant glutamine residue that is critical for substrate and inhibitor binding. PDE4C appears to be more distal from other PDE4 subfamilies, with certain key residues being disordered. Our analyses provide the first structural basis for the development of PDE4 subfamily-selective inhibitors.

Key words: cAMP phosphodiesterase, 4-[8-(3-nitrophenyl)-[1,7]-naphthyridin-6-yl]benzoic acid (NVP), phosphodiesterase-4 crystal structure, phosphodiesterase-4 inhibitor.

## INTRODUCTION

Cyclic nucleotide PDEs (phosphodiesterases) hydrolyse the second messengers cAMP and cGMP, which act as key regulators of many important physiological processes [1–4]. PDEs provide the sole means of inactivating these cyclic nucleotides and thus play pivotal regulatory roles. The human genome encodes 21 PDE genes that are categorized into 11 families. Alternative mRNA splicing of the 21 genes generates approx. 100 isoforms of PDEs in various human tissues. The conservation of these genes implies important physiological functions.

PDE family-selective inhibitors have been widely studied as therapeutics, including cardiotonic agents, vasodilators, smooth muscle relaxants, antidepressants, anti-thrombotics, anti-asthmatics and agents for treatment of COPD (chronic obstructive pulmonary disease) and for improvement of learning and memory [5–10]. The PDE5 selective inhibitors sildenafil (Viagra), vardenafil (Levitra) and tadalafil (Cialis) are the best known examples and have been successfully deployed as therapeutics for treatment of male erectile dysfunction. PDE4-selective inhibitors form the largest group of molecules that have been developed among any PDE families. These inhibitors have been extensively studied as anti-inflammatory therapeutics for treatment of asthma and COPD, and also for rheumatoid arthritis, multiple sclerosis, Type 2 diabetes, septic shock, leukaemia, atopic dermatitis and other autoimmune diseases [9–12]. More recently, there has been rekindling of interest in the potential use of PDE4-selective inhibitors for treating both depression and affective disorders such as schizophrenia [13,14].

The obstacles preventing PDE4 inhibitors from practical application are side effects such as nausea and emesis, which limit the effective therapeutic window [10–12]. Although the exact mechanisms underpinning the side effects of current PDE4-selective inhibitors are unclear, one source is thought to be their non-selective inhibitory effects on the four PDE4 subfamilies (A, B, C and D) [9]. This concept has gained considerable support from the studies on both targeted knockout of specific PDE4 genes in mice, cell-based analysis of siRNA (small interfering RNA)-mediated knockdown of specific PDE4 subfamilies and dominant-negative strategies [15–20]. These studies have identified unique non-redundant roles for PDE4 subfamilies and isoforms, indicating that PDE4 subfamily-selective inhibitors may offer a route for maximizing therapeutic actions while minimizing side effects. The abundance of PDE4B in neutrophils and monocytes [21], coupled with targeted gene knockout studies [15,17], suggests that PDE4B is the likely target for the anti-inflammatory actions of PDE4-selective inhibitors. This argument is supported by the observations that anti-inflammatory activity is correlated with the inhibition of PDE4A and PDE4B [16,22] and is unaffected in mice with PDE4D gene knockout [23]. In addition, studies on PDE4D-knockout mice suggest that PDE4D may be connected with the central-nervous-system-related emetic [24] and cardiac [25] side effects. On the other hand, PDE4D has recently been shown to play a predominant

Abbreviations used: COPD, chronic obstructive pulmonary disease; ERK, extracellular-signal-regulated kinase; NVP, 4-[8-(3-nitrophenyl)-[1,7]naphthyridin-6-yl]benzoic acid; PDE, phosphodiesterase; PEG, poly(ethylene glycol); PKA, protein kinase A; RMSD, root mean square deviation; UCR, upstream conserved regulatory region.

[1] Correspondence may be addressed to either of these authors (email puscjw@mail.sysu.edu.cn or hke@med.unc.edu).

Structural co-ordinates have been deposited in the RCSB Protein Data Bank under accession codes 2QYK (PDE4A10 in complex with NVP), 2QYL (PDE4B2B in complex with NVP), 2QYM (unliganded PDE4C2) and 2QYN (PDE4D2 in complex with NVP).

role in T-cell proliferation [26], implying irreplaceable roles of individual PDE4 subfamilies in cellular processes and the therapeutic value of PDE4 subfamily-selective inhibitors.

Some attempts have been made to develop PDE4 inhibitors that selectively discriminate between the four PDE4 subfamilies in the anticipation that they will have less severe side effects. However, only very few PDE4 subfamily-selective inhibitors have been reported to date [27,28], probably due to the lack of comparative structural information for the active sites of the four PDE4 subfamilies. An example of a PDE4 subfamily selective inhibitor is NVP {4-[8-(3-nitrophenyl)-[1,7]naphthyridin-6-yl]benzoic acid}, which has been demonstrated to show selectivity for PDE4D (88-, 49- and 68-fold compared with PDE4A, PDE4B and PDE4C respectively) [27]. Although various structures of PDE4B and PDE4D in complex with inhibitors are available [29], no structures of PDE4A, PDE4C or any PDE4 complexes with subfamily-selective inhibitors have been reported. The present paper addresses these important deficiencies and reports the crystal structures of the catalytic domains of PDE4A, PDE4B and PDE4D in complex with the selective inhibitor NVP, as well as the structure of the unliganded PDE4C at high resolution. These structures show that NVP binds to the deep pocket of the active site and causes subtle, but significant, changes in the conformation of the active sites of the PDE4 subfamilies.

## MATERIALS AND METHODS

### Subcloning, expression and purification of PDE catalytic domains

The EST (expressed sequence tag) cDNA clones of PDE4A10 (GenBank® accession number AF073745), PDE4B2B (GenBank® accession number XM_001862) and PDE4D2 (GenBank® accession number AF012074) were purchased from the A.T.C.C. (Manassas, VA, U.S.A.). The human PDE4C2 was reported previously [30]. The cDNAs for expression of the catalytic domains of PDE4A10 (residues 290–622), PDE4B2B (residues 152–487), PDE4C2 (residues 200–558) and PDE4D2 (residues 86–413) were subcloned into the expression vector pET15b. The resultant plasmids pET-PDE4A, pET-PDE4B, pET-PDE4C and pET-PDE4D were transferred into *Escherichia coli* strain BL21 (Codonplus) cells for overexpression. The *E. coli* cells carrying the plasmids were grown in LB (Luria–Bertani) medium at 37 °C to a $D_{600}$ of 0.7 and then 0.1 mM IPTG (isopropyl $\beta$-D-thiogalactoside) was added to induce overexpression at 15 °C for 20–40 h. The recombinant proteins of PDE4A10, PDE4B2B, PDE4C2 and PDE4D2 were passed through an Ni-NTA ($Ni^{2+}$-nitrilotriacetate) column (Qiagen), followed by thrombin cleavage, and purified further using columns of Q-Sepharose (Amersham Biosciences) and Sephacryl S300 (Amersham Biosciences). A typical batch of purification yielded approx. 10 mg of PDE4A10, 20 mg of PDE4B2B, 10 mg of PDE4C2 and 100 mg of PDE4D2 from 2 litres of cell culture. The purified PDE4 proteins showed a single band by SDS/PAGE and are estimated to have a purity of > 95 %.

### Protein crystallization and structural determination

All of the crystals of PDE4 subfamilies in complex with NVP were grown by vapour diffusion. The PDE4–NVP complexes were prepared by mixing 50 mg/ml PDE4A10-(290–622), 26 mg/ml PDE4B2B-(150–487) or 30 mg/ml PDE4D2 with 4 mM NVP. The protein drops consisted of 2 $\mu$l of complex solution and 2 $\mu$l of well buffer: 12 % PEG [poly(ethylene glycol)] 400, 200 mM magnesium acetate, 0.1 M Tris/HCl (pH 8.5) and 5 % glycerol at 4 °C for PDE4A10; 12 % PEG3350, 0.1 M Tris/HCl (pH 8.5), 35 % ethylene glycol and 200 mM $MgCl_2$ at 25 °C for PDE4B2B; and 18 % PEG3350, 0.1 Hepes (pH 7.5), 30 % ethylene glycol, 10 % propan-2-ol and 200 mM $MgCl_2$ at 4 °C for PDE4D2. The unliganded PDE4C2 at 15 mg/ml (residues 200–558) was crystallized by the hanging drop method against the well buffer of 10 % PEG3350, 100 mM $MgCl_2$ and 0.1 M Hepes (pH 7.5) at 25 °C.

The diffraction data were collected in beamline X29 of Brookhaven National Laboratory and processed by the program HKL (Table 1) [31]. The structures were solved by molecular replacement [32], using the known PDE4D or PDE4B structure as the initial model. The phases from the molecular replacement were improved by the density modification package of the CCP4. The structures were rebuilt by the program O [33] and refined by the program CNS (Table 1) [34].

### Synthesis of the PDE4 selective inhibitor NVP

NVP (Figure 1, left-hand panel) was synthesized by following the protocol of Hersperger et al. [27], and confirmed by $^1$H-NMR {(300 MHz, [$^2H_6$]DMSO) $\delta$ 9.09 (m, 2H), 8.69 (m, 2H), 8.64 (dd, 1H), 8.40 (m, 3H), 8.11 (d, 2H), 7.87 (m, 2H)] and mass spectrum [($m/z$) $[M+H]^+$ 372}.

### Assay of phosphodiesterase activities

The PDE4 enzymes were incubated with a reaction mixture containing 20 mM Tris/HCl (pH 7.5), 10 mM $MgCl_2$, 1 mM dithiothreitol and [$^3$H]cAMP or [$^3$H]cGMP (20 000 c.p.m./assay) at room temperature (25 °C) for 15 min. The reactions were terminated by addition of 0.2 M $ZnSO_4$ and 0.2 M $Ba(OH)_2$. The reaction products [$^3$H]AMP or [$^3$H]GMP were precipitated by $BaSO_4$, while unreacted [$^3$H]cAMP or [$^3$H]cGMP remained in the supernatant. Radioactivity in the supernatant was measured by liquid-scintillation counting. The enzymatic activity was measured at eight concentrations of cAMP and cGMP with two or three repeats. For measurement of inhibition, 11 or 12 concentrations of inhibitors were used, together with the substrate concentration of one-tenth of the $K_m$ and the enzyme concentration for 50 % hydrolysis of substrates. The kinetic parameters $K_m$ and $k_{cat}$ were obtained following the theory of steady-state kinetics.

## RESULTS

### Enzymatic properties of the PDE4 catalytic domain

Since PDE4 isoforms differ only in their N-terminal regions, the isoforms PDE4A10 (residues 290–622), PDE4B2B (residues 152–487), PDE4C2 (residues 200–558) and PDE4D2 (residues 86–413) reflect their core PDE4 subfamily catalytic domains. As such, we will refer to these as PDE4A, PDE4B, PDE4C and PDE4D, but keep the residue numbering for the particular isoforms.

Assayed with their substrate cAMP, the functional PDE4A, PDE4B, PDE4C and PDE4D catalytic domains exhibited $K_m$ values of 0.8–5.1 $\mu$M and $k_{cat}$ values of 0.7–6.7 $s^{-1}$ (Table 2). These $K_m$ values for the catalytic domains are comparable with $K_m$ values of 1–6 $\mu$M for the full-length proteins of the PDE4 subfamilies in the literature [1,21,30,35]. The catalytic domain derived from PDE4D2 has $k_{cat}/K_m$ of 3.5 $s^{-1} \cdot \mu M^{-1}$, and is approx. 10-fold more efficient than the catalytic domain of PDE4B. Using cGMP as a substrate, PDE4C and PDE4D have $K_m$ values of 0.24 and 0.43 mM, and $k_{cat}$ values of 0.48 and 1.2 $s^{-1}$ respectively. However, the kinetic parameters for PDE4A and PDE4B could not be measured accurately, because of the limited solubility of cGMP under the assay conditions (Table 2). The substrate specificity

**Table 1 Diffraction data and structural refinement statistics**

(a) Data collection

| Parameter | PDE4A–NVP | PDE4B–NVP | PDE4C native | PDE4D–NVP |
|---|---|---|---|---|
| Space group | $P4_12_12$ | $C222_1$ | $P6_122$ | $P2_12_12_1$ |
| Unit cell (*a*, *b*, *c*, Å) | 105.4, 105.4, 166.1 | 91.8, 105.4, 87.8 | 74.7, 74.7, 275.9 | 58.1, 80.6, 163.3 |
| Resolution (Å) | 2.1 | 1.95 | 1.90 | 1.57 |
| Total measurements | 1479463 | 375717 | 1448275 | 793901 |
| Unique reflections | 55625 | 28299 | 36952 | 103916 |
| Completeness (%) | 100.0(100.0)* | 89.8 (61.6) | 99.9 (99.9) | 96.4 (72.0) |
| Average $I/\sigma$ | 9.5 (5.0)* | 13.7 (5.0) | 8.7 (4.1) | 16.1 (2.4) |
| $R_{merge}$ | 0.091 (0.53)* | 0.064 (0.32) | 0.095 (0.63) | 0.054 (0.38) |

(b) Structural refinement

| Parameter | PDE4A–NVP | PDE4B–NVP | PDE4C native | PDE4D–NVP |
|---|---|---|---|---|
| *R*-factor | 0.201 | 0.213 | 0.208 | 0.225 |
| *R*-free | 0.234 (10%)† | 0.239 (10%) | 0.229 (10%) | 0.248 (10%) |
| Resolution (Å) | 30–2.1 | 30–1.95 | 30–1.9 | 30–1.57 |
| Reflections | 53788 | 27655 | 36109 | 99820 |
| RMSD | | | | |
| Bond (Å) | 0.006 | 0.006 | 0.005 | 0.005 |
| Angle (°) | 1.10 | 1.07 | 1.06 | 1.04 |
| Average *B*-factor (Å$^2$) | | | | |
| Protein | 37.4 (5404)‡ | 42.9 (2707) | 32.6 (2332) | 26.3 (5271) |
| NVP | 71.7 (56) | 45.1 (28) | | 26.3 (56) |
| Water molecules | 39.1 (269)‡ | 41.5 (68) | 36.2 (127) | 32.696 (365) |
| Zn | 31.1 (2)‡ | 38.2 (1) | 25.2 (1) | 16.5 (2) |
| Mg | 35.2 (2)‡ | 42.1 (2) | 24.3 (1) | 13.8 (2) |

* The numbers in parentheses are for the highest resolution shell.
† The percentage of reflections omitted for calculation of *R*-free.
‡ The number of atoms in the crystallographic asymmetric unit.

**Table 2 Kinetic parameters of PDE4**

The apparent $K_m$ and $k_{cat}$ values were determined from Eadie–Hofstee plots of $v_0$ against $v_0$/[S]. Each value was measured at least twice. Protein concentrations were converted from the $\varepsilon_{280}$ molar absorption coefficient calculated by the ProtParam program.

| | $K_m^{cAMP}$ ($\mu$M) | $k_{cat}^{cAMP}$ ($s^{-1}$) | $(k_{cat}/K_m)^{cAMP}$ ($s^{-1} \cdot \mu M^{-1}$) | $K_m^{cGMP}$ ($\mu$M) | $k_{cat}^{cGMP}$ ($s^{-1}$) | $(k_{cat}/K_m)^{cGMP}$ ($s^{-1} \cdot \mu M^{-1}$) | $(k_{cat}/K_m)^{cAMP}/(k_{cat}/K_m)^{cGMP}$ | $IC_{50}$ of NVP ($\mu$M) |
|---|---|---|---|---|---|---|---|---|
| PDE4A | 5.1 ± 0.5 | 6.7 ± 0.2 | 1.3 ± 0.2 | > 1000 | – | – | – | 3.3 ± 0.2 |
| PDE4B | 4.5 ± 0.3 | 1.56 ± 0.05 | 0.35 ± 0.03 | > 1000 | – | – | – | 0.65 ± 0.01 |
| PDE4C | 0.80 ± 0.14 | 0.66 ± 0.05 | 0.85 ± 0.18 | 240 ± 55 | 0.48 ± 0.10 | $2.0 \pm 0.04 \times 10^{-3}$ | 427 | 5.7 ± 0.2 |
| PDE4D | 1.5 ± 0.1 | 5.4 ± 1.0 | 3.5 ± 0.7 | 427 ± 23 | 1.19 ± 0.02 | $2.8 \pm 0.1 \times 10^{-3}$ | 1250 | 0.57 ± 0.04 |

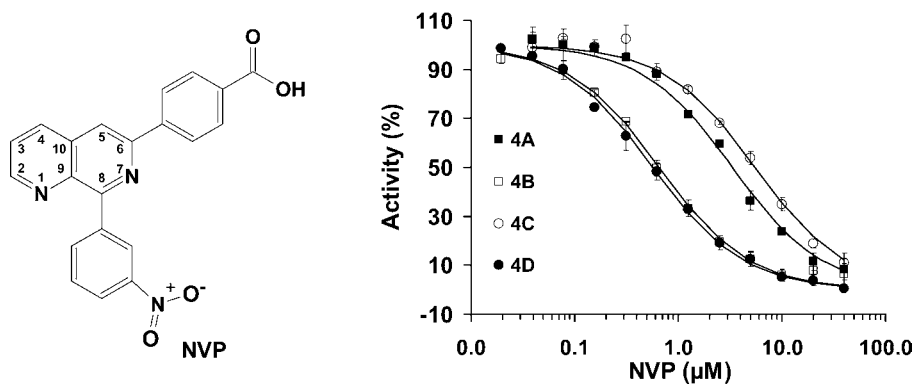


**Figure 1 Inhibition of PDE4 subfamilies by NVP**

Left: chemical structure of NVP. Right: inhibition of NVP on PDE4A (■), PDE4B (□), PDE4C (○) and PDE4D (●). Results are means ± S.D. of two or three repeated measurements. A substrate concentration of 0.04 $\mu$M cAMP was used in the determination of the $IC_{50}$ values.

constants of $(k_{cat}/K_m)^{cAMP}/(k_{cat}/K_m)^{cGMP}$ are 427 and 1250 for the catalytic domains of PDE4C and PDE4D, thus indicating their cAMP specificity. Although the $k_{cat}$ values for cGMP and cAMP are similar among the PDE4 subfamilies, the $K_m$ values are dramatically different for these two substrates. This suggests that the cAMP preference of the PDE4 proteins is determined by the poor affinity of cGMP.

The $IC_{50}$ values for NVP are 3.3, 0.65, 5.7 and 0.57 $\mu$M for PDE4A, PDE4B, PDE4C and PDE4D respectively (Figure 1, right-hand panel, and Table 2). Thus the potency of NVP inhibition on PDE4D and PDE4B is similar, but approx. 10-fold better than that of PDE4C. Our data concerning the NVP inhibition of the catalytic domains of each of the four PDE4 subfamilies are significantly different from the earlier reported values of 88, 49, 68 and 1 nM for PDE4A, PDE4B, PDE4C and PDE4D respectively [27]. The explanation for this disagreement is not clear, but there are two possibilities. First, our data were measured against the defined catalytic domains of the PDE4 subfamilies, in contrast with undefined full-length proteins expressed in *Saccharomyces cerevisiae* in the earlier study [27]. Thus the high selectivity against the full-length PDE4D might represent the contribution of the N- or C-terminal regions of the PDE4 subfamilies, although the catalytic domains of the PDE families such as 4, 7 and 10 have been reported to have $K_m$ and kinetic parameters comparable with those of the full-length proteins [35,36]. On the other hand, the use of partially purified proteins in the earlier study may affect the accuracy of the measurements. In this regard, it has been shown that certain proteins can interact with full-length PDE4 isoforms and modify their function [37]. It has also been reported that the full-length PDE4D3 protein used in the analyses by Hersperger et al. [27] can be modified in its UCR (upstream conserved regulatory region) 1 by PKA (protein kinase A) phosphorylation, so that its sensitivity to certain PDE4-selective inhibitors can be altered [38]. Thus any 'impurities' in their assay systems might have an impact on the protein activity or the measurement accuracy.

### Structural architecture

The crystallographic asymmetric units contain two catalytic domains of PDE4A–NVP and PDE4D–NVP, but one of PDE4B–NVP and unliganded PDE4C. The entire catalytic domains of PDE4A10 (residues 298–622), PDE4B2B (residues 152–487) and PDE4D2 (residues 86–411), and the core domain of PDE4C2 (residues 201–332, 346–464 and 491–536) are unambiguously traced in the structures (Figure 2). Residues 333–345 of the H-loop and 465–490 of the M-loop in PDE4C lacked electron density and are disordered. All four structures of the PDE4 subfamilies have the same folding and secondary structures. This is not surprising because the catalytic domains of the PDE4 subfamilies have a high degree of amino acid conservation, in which 254 out of 325 residues (78 %) are identical. The superposition of PDE4D on PDE4A, PDE4B and PDE4C yielded RMSDs (root mean square deviations) of 0.67, 0.73 and 0.64 Å (1 Å = 0.1 nm) respectively for the $C^{\alpha}$ atoms of the comparable residues in the domains, indicating the overall similarity of the catalytic domain in the PDE4 subfamilies.

The catalytic domains of the PDE4 subfamilies contain 16 $\alpha$-helices (Figure 2), as reported previously [39]. However, helices H8 and H9 of the H-loop, six tail residues of H14, and four head residues of H15 in PDE4C are disordered. The catalytic pocket can be divided further into two major sub-pockets for binding of bivalent metals and substrates. The metal-binding pocket contains two bivalent metal ions: a zinc ion that has been confirmed by the anomalous scattering, together with an unidentified bivalent metal, presumed to be magnesium, which has been shown to be important for catalytic activity [4,38,40]. A magnesium ion was thus used as the second metal in the refinement of all the four structures and shows a comparable *B*-factor under full occupancy (Table 1). Both metal ions form six co-ordinations in an octahedral configuration. Zinc co-ordinates with $His^{164}$, $His^{200}$, $Asp^{201}$, $Asp^{318}$ and two water molecules in the PDE4D–NVP structure, whereas magnesium interacts with $Asp^{201}$ and five waters molecules. The metal co-ordination in PDE4A, PDE4B and PDE4C is the same as that in PDE4D.

### Binding of NVP

The inhibitor NVP binds to the active sites of PDE4A, PDE4B and PDE4D with a similar conformation (Figure 3). The electron-density maps reveal unambiguously the binding position and conformation of NVP, although its nitrate group has relatively weaker density (Figure 3). The carboxyphenyl and naphthyridine groups form almost a co-plane with an approx. 10° tilt, whereas the nitrophenyl group is approx. 40° off the naphthyridine plane (Figures 3D and 3E). The *B*-factors of NVPs are comparable with the average of the protein atoms in the PDE4B and PDE4D structures (Table 1), suggesting its full occupancy. However, the B-factor of NVP in the PDE4A structure is significantly higher (Table 1), implying its partial occupancy. In order to assess the interaction of NVP with PDE4 subfamily members, we describe its binding to PDE4D in detail and then compare, where appropriate, its interaction with other PDE4 subfamilies.

NVP forms only one hydrogen bond between its N1 and Ne2 of the invariant glutamine at the active site of all PDE4 subfamilies ($Gln^{369}$ in PDE4D, Figure 4). NVP is partially buried within the pocket and has a solvent-accessible area of approx. 10 % in all three PDE4–NVP complex structures. The naphthyridine group is completely buried and not accessible. The carboxyphenyl group orients to the metal-binding pocket and forms hydrogen bonds with five water molecules, two of which are metal-bound. The nitrophenyl group of NVP orients its nitrate group towards the surface of the PDE4 molecules, but, surprisingly, no water binds to the nitrate groups in most of the PDE4 subfamilies, except one in the PDE4B structure. A key feature seen in all examples of NVP binding to the PDE4 subfamilies is its tilted stacking against the conserved phenylalanine residue ($Phe^{372}$ in PDE4D) located in the active site. In most structures of the PDE–inhibitor complexes, the conserved phenylalanine residue stacks in parallel to either a benzene group, such as is found in rolipram with PDE4, or a hydrophobic ring, such as pyrazolopyrimidinone of sildenafil in the PDE5A1 structure [29]. However, the nitrophenyl group and the naphthyridine ring of NVP share the interaction with the conserved phenylalanine residue, resulting in a tilt to each ring plane. In addition, NVP forms van der Waals interactions with $Tyr^{159}$, $Met^{273}$, $Asn^{321}$, $Ile^{336}$, $Phe^{340}$, $Met^{357}$ and $Ser^{368}$ in PDE4D. All of these residues are identical across the four PDE4 subfamilies.

### Subtle, but significant, differences at the active sites of PDE4 subfamilies

In spite of such overall similarity, structural superposition shows subtle, but significant, differences at the active sites of the PDE4 subfamilies. Among the PDE4 subfamilies, PDE4B and PDE4D are most comparable. Thus almost all the residues of PDE4B and PDE4D that are involved in inhibitor binding have the same conformation with small positional differences. $Met^{451}$ of PDE4B, which connects with helices H14 and H15, is a clear exception, as it exhibits significant conformational changes from $Met^{357}$ of PDE4D (Figure 4c). Since this methionine residue has

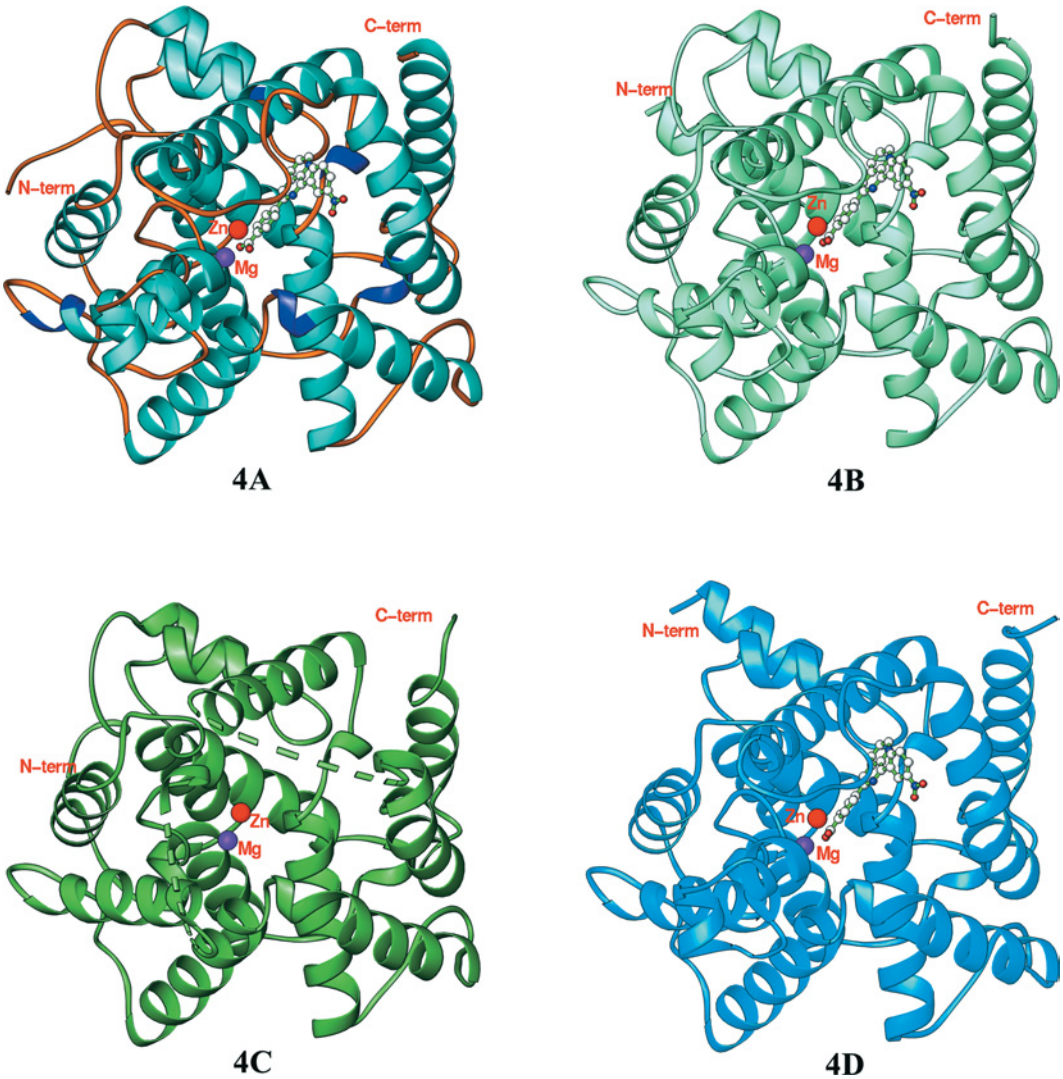


**Figure 2 Ribbon diagrams of PDE4 subfamily members 4A, 4B, 4C and 4D**

The broken lines in PDE4C represent the disordered residues 333–345 of the H-loop and 465–490 of the M-loop. C-term, C-terminus; N-term, N-terminus.

relatively larger *B*-factors (47.7, 60.6 and 43.8 compared with 37.4, 42.9 and 26.3 Å$^2$ of overall averages in PDE4A, PDE4B and PDE4D respectively), its position is more flexible. Although the conformational changes of the methionine residue would be expected to have an impact on the inhibitor binding, there may be other unidentified elements that compromise this effect. Thus these comparative studies imply that the catalytic domains of PDE4B and PDE4D are likely to have similar affinities for competitive inhibitors.

The structural superposition of PDE4A on PDE4D shows more divergence than PDE4B, as indicated by average displacement of 0.34 Å for C$^\alpha$ of 15 active-site residues of PDE4A and PDE4D compared with 0.24 Å for those of PDE4B and PDE4D. In addition, Ala$^{363}$–Ser$^{368}$ of PDE4D show an average positional shift of 1.1 Å for the C$^\alpha$ atoms of their equivalents in PDE4A, which is about twice the overall average between the structures of PDE4A and PDE4D. Since these residues are next to the invariant Gln$^{369}$ that is critical for binding of inhibitors and substrates, such a positional shift would be expected to affect the binding affinity of inhibitors.

The positional difference between residues of PDE4C and PDE4D are more obvious. This is shown in Figure 4(D) and also by the average displacement of 0.49 Å for the C$^\alpha$ atoms of 12 active site residues between PDE4C and PDE4D. In addition, the conformation of the side chain of Phe$^{340}$ of PDE4D swings to a different direction from that observed in PDE4C. Furthermore, the majority of the residues in the H- and M-loops, which are important for inhibitor binding, are disordered in PDE4C. Although the structure PDE4C in complex with NVP is not available, we believe that the conformation of the unliganded PDE4C simulates that in the complex state because the conformations of the unliganded PDE4B and PDE4D are very similar to the NVP- and other inhibitor-bound states, as shown by the structure superposition. Therefore these observations imply that the catalytic site of PDE4C is unique among PDE4 subfamilies, but those of the PDE4B and PDE4D can be categorized together. In short, the structural studies suggest that it may be relatively easier to develop PDE4C-selective inhibitors, but more difficult to obtain inhibitors with PDE4B and PDE4D selectivity.

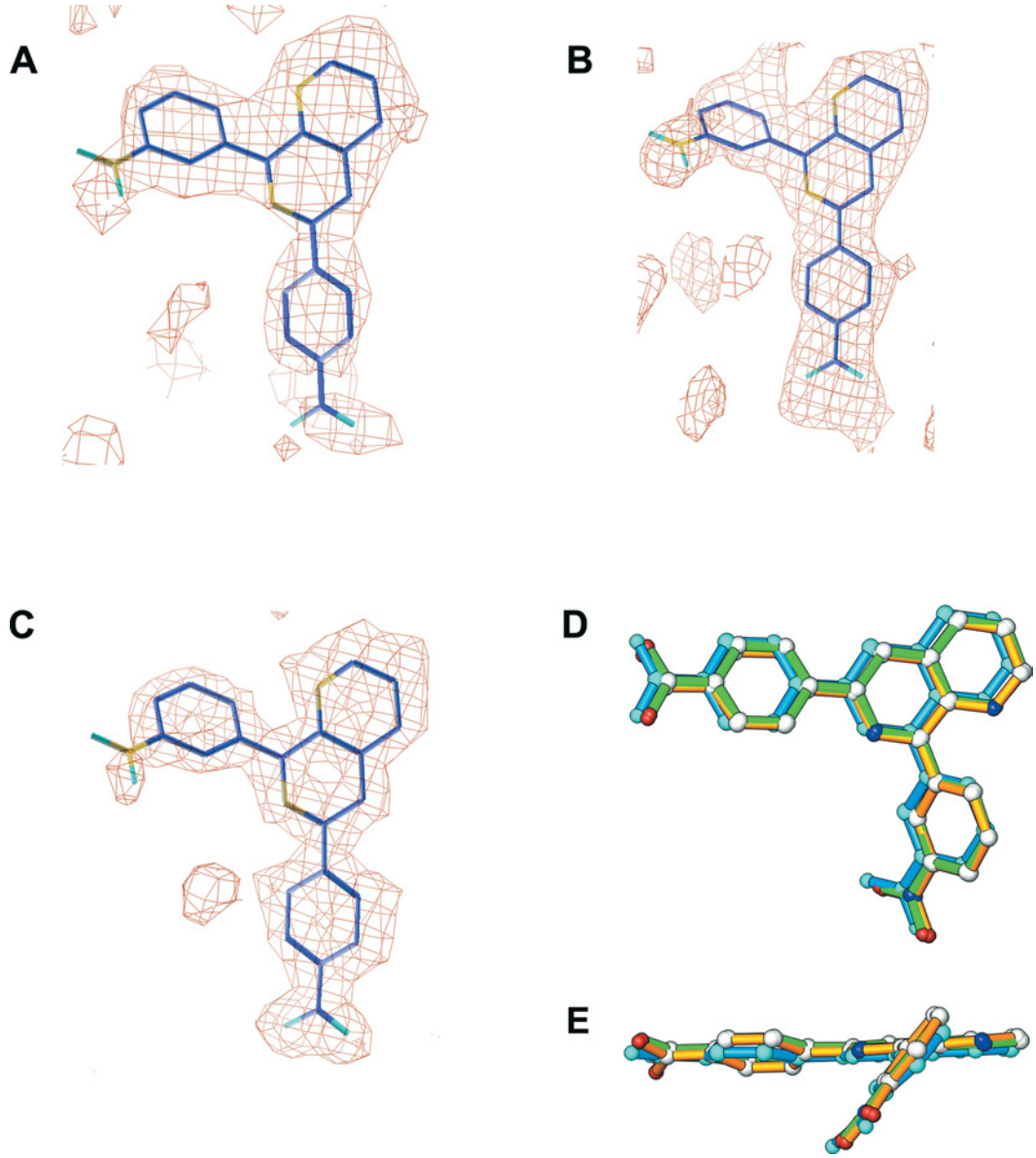


**Figure 3 Conformation of NVP**

(**A**) Electron density map for inhibitor NVP. The $F_o-F_c$ map was calculated from the PDE4A10 structure with omission of NVP and contoured at $2\sigma$. (**B**) The PDE4B2B map was contoured at $2\sigma$. (**C**) The PDE4D2 map was contoured at $2.5\sigma$. (**D**) Superposition of NVPs from PDE4A (cyan), PDE4B (green) and PDE4D (gold). (**E**) A 90° view of the NVP superposition from (**D**).

## DISCUSSION

### Implications of the subfamily selectivity of PDE4 inhibitors

Although poor subfamily-selectivity of PDE4 inhibitors is thought to be one possible cause of their side effects, only a few subtype-selective PDE4 inhibitors that exhibit a limited degree of selectivity for PDE4D have been reported [22,27,28]. The structures of the PDE4 subfamilies in complex with NVP provide an explanation to why it is so difficult to develop PDE4 subfamily-selective inhibitors. First, residues that are involved in direct interaction with NVP or located at the second shell of the active site are identical in all the PDE4 subfamilies. This suggests a similar energy for inhibitor binding. Secondly, structural superposition reveals that the active site has a similar conformation and pocket size in all of the four PDE4 subfamilies. Thirdly, the deeply buried pocket available for inhibitor binding within the active site implies that the pocket itself dominates subfamily selectivity. These observations imply severe limitations for development of active-site-directed PDE4 subfamily inhibitors.

On the other hand, our comparative structural studies identify, for the first time, subtle, but significant, differences in the active site of the PDE4 subfamilies. Indeed, PDE4A shows the significant displacement of the N-terminal residues ($Ala^{575}$–$Ser^{580}$) of the invariant glutamine residue ($Gln^{581}$) that is critical for binding of both substrates and inhibitors, and several of the active-site residues of PDE4C are disordered. These structural differences potentially provide a new basis for the design of novel classes of PDE4 subfamily-selective inhibitors.

We also note that other factors in full-length PDE4 isoforms may impinge on the function and structure of the catalytic unit

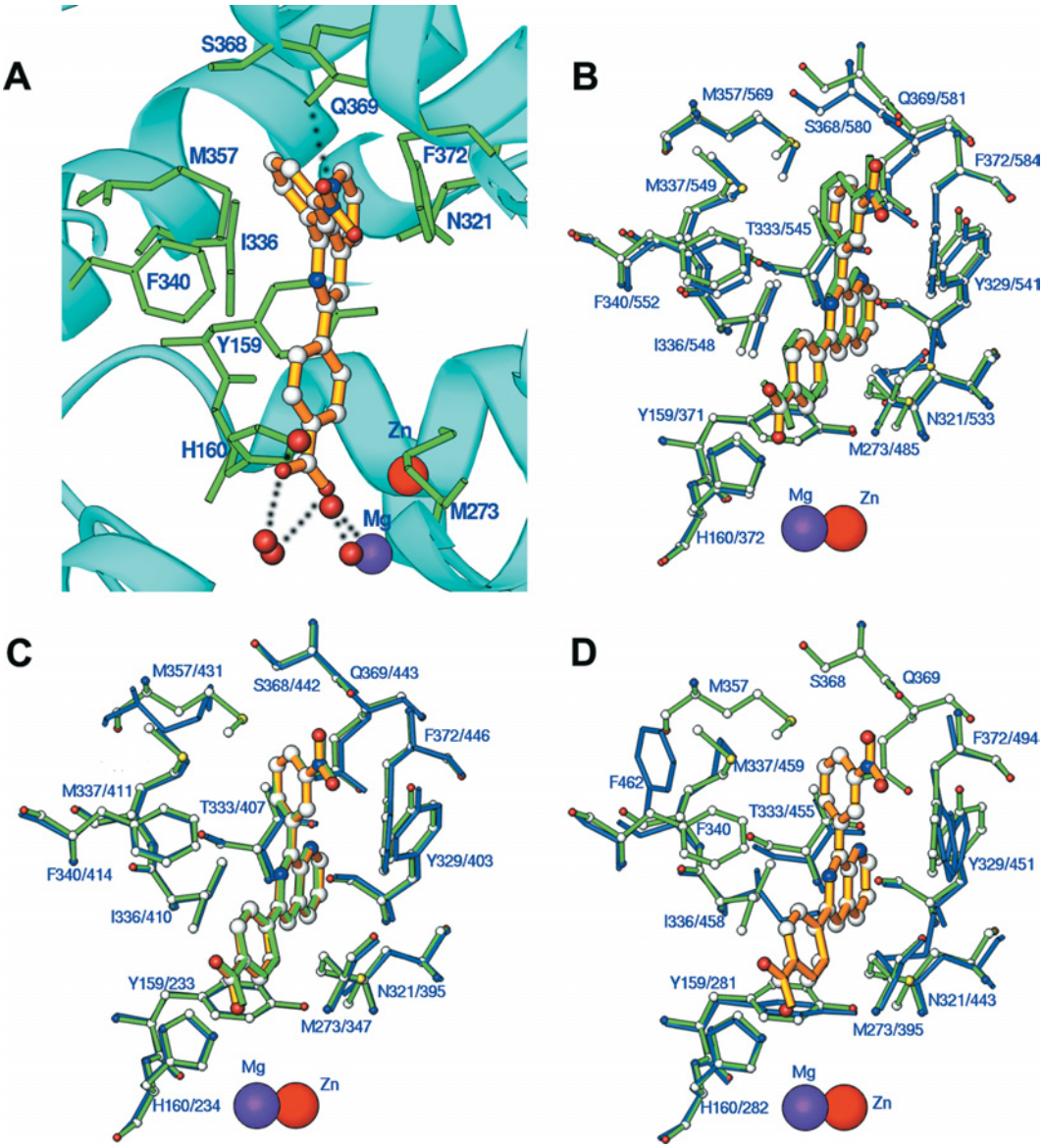


**Figure 4 Binding of NVP to the PDE4 subfamilies**

(**A**) The interaction of NVP (golden bonds) with the PDE4D2 residues (green bonds). Broken lines represent the hydrogen bonds or metal co-ordination. (**B**) Superposition of PDE4A10–NVP (blue and orange bonds) on PDE4D2–NVP (green bonds). Residue numbers, such as M357/569, are those of PDE4D2/PDE4A10 respectively. $Ser^{368}$ of PDE4D2 shows a significant shift from $Ser^{580}$ of PDE4A10. (**C**) Superposition of PDE4B2B–NVP (blue and orange) on PDE4D2–NVP (green). (**D**) Superposition of PDE4C2 (blue) on PDE4D2–NVP (green and orange). Residues $Met^{479}$, $Ser^{490}$ and $Gln^{491}$ of PDE4C2 are disordered and are not shown. Significant conformational changes are visible between PDE4C and PDE4D. For example, the side-chain $Phe^{340}$ of PDE4D2 has a different orientation from $Phe^{462}$ of PDE4C2.

and may also be usefully exploited in developing other classes of PDE4-selective inhibitors. Thus the UCR1 and UCR2 domains, which are located immediately N-terminal to the catalytic unit, act to direct the functional changes in PDE4 catalytic activity, presumably due to altered conformation of the PDE4 catalytic domain upon phosphorylation by PKA [41], ERK (extracellular-signal-regulated kinase) [42] and a kinase downstream of PI3K (phosphoinositide 3-kinase) [43]. Indeed, PKA phosphorylation of PDE4D3, which is mediated via UCR1, has been shown to lead to alterations in sensitivity to inhibition of rolipram [38,41]. In addition, the binding of XAP2 (X-associated protein 2)/AIP (aryl hydrocarbon receptor-interacting protein) to PDE4A5 has been shown to regulate the catalytic activity of this isoform [37]. Other proteins such as ERK2 [42], $\beta$-arrestin [44] and AKAP18 (A-kinase-anchoring protein 18) [45] also bind to the PDE4 catalytic unit and may effect subtle conformational changes. These proteins may interact directly with the surface residues of the pocket, such as $Ser^{226}$ of the H-loop and $Arg^{342}$ of the M-loop in PDE4D, thus affecting the inhibitor selectivity.

The present study provides the first structural insights into the catalytic domains of PDE4A and PDE4C coupled with the first structural evaluation of PDE4 catalytic units in complex with a subfamily-selective inhibitor. These structures may lead to the development of strategies that might be adopted to design subfamily-selective inhibitors. The structural information of the

present study also indicates the likelihood of changes occurring in the conformation of the active site through protein–protein interactions and through the action of the UCR1 and UCR2 modules.

We thank Beamline X29 at NSLS (National Synchrotron Light Source) for collection of diffraction data. This work was supported by NIH (National Institutes of Health) grant GM59791 to H.K., Medical Research Council (U.K.) grants (G8604010 and G0400053) and European Union Grant (037189) to M.D.H., and the 985 project of Sun Yat-Sen University.

## REFERENCES

1 Bender, A. T. and Beavo, J. A. (2006) Cyclic nucleotide phosphodiesterases: molecular regulation to clinical use. Pharmacol. Rev. **58**, 488–520
2 Lugnier, C. (2006) Cyclic nucleotide phosphodiesterase (PDE) superfamily: a new target for the development of specific therapeutic agents. Pharmacol. Ther. **109**, 366–398
3 Omori, K. and Kotera, J. (2007) Overview of PDEs and their regulation. Circ. Res. **100**, 309–327
4 Conti, M. and Beavo, J. (2007) Biochemistry and physiology of cyclic nucleotide phosphodiesterases: essential components in cyclic nucleotide signaling. Annu. Rev. Biochem. **76**, 481–511
5 Rotella, D. P. (2002) Phosphodiesterase 5 inhibitors: current status and potential applications. Nat. Rev. Drug Discov. **1**, 674–682
6 Menniti, F. S., Faraci, W. S. and Schmidt, C. J. (2006) Phosphodiesterases in the CNS: targets for drug development. Nat. Rev. Drug Discov. **5**, 660–670
7 Castro, A., Jerez, M. J., Gil, C. and Martinez, A. (2005) Cyclic nucleotide phosphodiesterases and their role in immunomodulatory responses: advances in the development of specific phosphodiesterase inhibitors. Med. Res. Rev. **25**, 229–244
8 Blokland, A., Schreiber, R. and Prickaerts, J. (2006) Improving memory: a role for phosphodiesterases. Curr. Pharm. Des. **12**, 2511–2523
9 Lipworth, B. J. (2005) Phosphodiesterase-4 inhibitors for asthma and chronic obstructive pulmonary disease. Lancet **365**, 167–175
10 Houslay, M. D., Schafer, P. and Zhang, K. Y. (2005) Phosphodiesterase-4 as a therapeutic target. Drug Discov. Today **10**, 1503–1519
11 Lerner, A. and Epstein, P. M. (2006) Cyclic nucleotide phosphodiesterases as targets for treatment of haematological malignancies. Biochem. J. **393**, 21–41
12 Huang, Z. and Mancini, J. A. (2006) Phosphodiesterase 4 inhibitors for the treatment of asthma and COPD. Curr. Med. Chem. **13**, 3253–3262
13 O'Donnell, J. M. and Zhang, H. T. (2004) Antidepressant effects of inhibitors of cAMP phosphodiesterase (PDE4). Trends Pharmacol. Sci. **25**, 158–163
14 Kanes, S. J., Tokarczyk, J., Siegel, S. J., Bilker, W., Abel, T. and Kelly, M. P. (2007) Rolipram: a specific phosphodiesterase 4 inhibitor with potential antipsychotic activity. Neuroscience **144**, 239–246
15 Ariga, M., Neitzert, B., Nakae, S., Mottin, G., Bertrand, C., Pruniaux, M. P., Jin, S. L. and Conti, M. (2004) Nonredundant function of phosphodiesterases 4D and 4B in neutrophil recruitment to the site of inflammation. J. Immunol. **173**, 7531–7538
16 Jin, S. L. and Conti, M. (2002) Induction of the cyclic nucleotide phosphodiesterase PDE4B is essential for LPS-activated TNF-$\alpha$ responses. Proc. Natl. Acad. Sci. U.S.A. **99**, 7628–7633
17 Jin, S. L., Lan, L., Zoudilova, M. and Conti, M. (2005) Specific role of phosphodiesterase 4B in lipopolysaccharide-induced signaling in mouse macrophages. J. Immunol. **175**, 1523–1531
18 Lynch, M. J., Baillie, G. S., Mohamed, A., Li, X., Maisonneuve, C., Klussmann, E., van Heeke, G. and Houslay, M. D. (2005) RNA silencing identifies PDE4D5 as the functionally relevant cAMP phosphodiesterase interacting with $\beta$-arrestin to control the protein kinase A/AKAP79-mediated switching of the $\beta_2$-adrenergic receptor to activation of ERK in HEK293B2 cells. J. Biol. Chem. **280**, 33178–33189
19 McCahill, A., McSorely, T., Huston, E., Hill, E. V., Lynch, M. J., Gall, I., Keryer, G., Lygren, B., Taskén, K., van Heeke, G. and Houslay, M. D. (2005) In resting COS1 cells a dominant negative approach shows that specific, anchored PDE4 cAMP phosphodiesterase isoforms gate the activation, by basal cyclic AMP production, of AKAP-tethered protein kinase A type II located in the centrosomal region. Cell. Signalling **17**, 1158–1173
20 Bolger, G. B., Baillie, G. S., Li, X., Lynch, M. J., Herzyk, P., Mohamed, A., Mitchell, L. H., McCahill, A., Hundsrucker, C., Klussmann, E. et al. (2006) Scanning peptide array analyses identify overlapping binding sites for the signalling scaffold proteins, $\beta$-arrestin and RACK1 in the cAMP-specific phosphodiesterase, PDE4D5. Biochem. J. **398**, 23–36
21 Wang, P., Wu, P., Ohleth, K. M., Egan, R. W. and Billah, M. M. (1999) Phosphodiesterase 4B2 is the predominant phosphodiesterase species and undergoes differential regulation of gene expression in human monocytes and neutrophils. Mol. Pharmacol. **56**, 170–174
22 Manning, C. D., Burman, M., Christensen, S. B., Cieslinski, L. B., Essayan, D. M., Grous, M., Torphy, T. J. and Barnette, M. S. (1999) Suppression of human inflammatory cell function by subtype-selective PDE4 inhibitors correlates with inhibition of PDE4A and PDE4B. Br. J. Pharmacol. **128**, 1393–1398
23 Hansen, G., Jin, S.-L. C., Umetsu, D. T. and Conti, M. (2000) Absence of muscarinic cholinergic airway responses in mice deficient in the cyclic nucleotide phosphodiesterase PDE4D. Proc. Natl. Acad. Sci. U.S.A. **97**, 6751–6756
24 Robichaud, A., Stamatiou, P. B., Jin, S. L., Lachance, N., MacDonald, D., Laliberte, F., Liu, S., Huang, Z., Conti, M. and Chan, C. C. (2002) Deletion of phosphodiesterase 4D in mice shortens $\alpha_2$-adrenoceptor-mediated anesthesia, a behavioral correlate of emesis. J. Clin. Invest. **110**, 1045–1052
25 Lehnart, S. E., Wehrens, X. H., Reiken, S., Warrier, S., Belevych, A. E., Harvey, R. D., Richter, W., Jin, S. L., Conti, M. and Marks, A. R. (2005) Phosphodiesterase 4D deficiency in the ryanodine-receptor complex promotes heart failure and arrhythmias. Cell **123**, 25–35
26 Peter, D., Jin, S. L., Conti, M., Hatzelmann, A. and Zitt, C. (2007) Differential expression and function of phosphodiesterase 4 (PDE4) subtypes in human primary $CD4^+$ T cells: predominant role of PDE4D. J. Immunol. **178**, 4820–4831
27 Hersperger, R., Bray-French, K., Mazzoni, L. and Muller, T. (2000) Palladium-catalyzed cross-coupling reactions for the synthesis of 6,8-disubstituted 1,7-naphthyridines: a novel class of potent and selective phosphodiesterase type 4D inhibitors. J. Med. Chem. **43**, 675–682
28 Chambers, R. J., Abrams, K., Castleberry, T. A., Cheng, J. B., Fisher, D. A., Kamath, A. V., Marfat, A., Nettleton, D. O., Pillar, J. D., Salter, E. D. et al. (2006) A new chemical tool for exploring the role of the PDE4D isozyme in leukocyte function. Bioorg. Med. Chem. Lett. **16**, 718–721
29 Ke, H. and Wang, H. (2007) Crystal structures of phosphodiesterases and implications on substrate specificity and inhibitor selectivity. Curr. Top. Med. Chem. **7**, 391–403
30 Owens, R. J., Lumb, S., Rees-Milton, K., Russell, A., Baldock, D., Lang, V., Crabbe, T., Ballesteros, M. and Perry, M. J. (1997) Molecular cloning and expression of a human phosphodiesterase 4C. Cell. Signalling **9**, 575–585
31 Otwinowski, Z. and Minor, W. (1997) Processing of X-ray diffraction data collected in oscillation mode. Methods Enzymol. **276**, 307–326
32 Navaza, J. and Saludjian, P. (1997) AMoRe: an automated molecular replacement program package. Methods Enzymol. **276**, 581–594
33 Jones, T. A., Zou, J.-Y., Cowan, S. W. and Kjeldgaard, M. (1991) Improved methods for building protein models in electron density maps and the location of errors in these models. Acta Crystallogr. Sect. A Found. Crystallogr. **47**, 110–119
34 Brünger, A. T., Adams, P. D., Clore, G. M., DeLano, W. L., Gros, P., Grosse-Kunstleve, R. W., Jiang, J. S., Kuszewski, J., Nilges, M., Pannu, N. S. et al. (1998) Crystallography and NMR system: a new software suite for macromolecular structure determination. Acta Crystallogr. Sect. D Biol. Crystallogr. **54**, 905–921
35 Wang, H., Liu, Y., Chen, Y., Robinson, H. and Ke, H. (2005) Multiple elements jointly determine inhibitor selectivity of cyclic nucleotide phosphodiesterases 4 and 7. J. Biol. Chem. **280**, 30949–30955
36 Wang, H., Liu, Y., Hou, J., Zheng, M., Robinson, H. and Ke, H. (2007) Structural insight into substrate specificity of phospodiesterase 10. Proc. Natl. Acad. Sci. U.S.A. **104**, 5782–5787
37 Bolger, G. B., Peden, A. H., Steele, M. R., MacKenzie, C., McEwan, D. G., Wallace, D. A., Huston, E., Baillie, G. S. and Houslay, M. D. (2003) Attenuation of the activity of the cAMP-specific phosphodiesterase PDE4A5 by interaction with the immunophilin XAP2. J. Biol. Chem. **278**, 33351–33363
38 Alvarez, R., Sette, C., Yang, D., Eglen, R. M., Wilhelm, R., Shelton, E. R. and Conti, M. (1995) Activation and selective inhibition of a cyclic AMP-specific phosphodiesterase, PDE-4D3. Mol. Pharmacol. **48**, 616–622
39 Xu, R. X., Hassell, A. M., Vanderwall, D., Lambert, M. H., Holmes, W. D., Luther, M. A., Rocque, W. J., Milburn, M. V., Zhao, Y., Ke, H. and Nolte, R. T. (2000) Atomic structure of PDE4: insight into phosphodiesterase mechanism and specificity. Science **288**, 1822–1825
40 Houslay, M. D. and Adams, D. R. (2003) PDE4 cAMP phosphodiesterases: modular enzymes that orchestrate signalling cross-talk, desensitisation and compartmentalization. Biochem. J. **370**, 1–18
41 Hoffmann, R., Wilkinson, I. R., McCallum, J. F., Engels, P. and Houslay, M. D. (1998) Cyclic AMP specific phosphodiesterase HSPDE4D3 mutants which mimic activation and changes in rolipram inhibition triggered by protein kinase A phosphorylation of $Ser^{54}$: generation of a molecular model. Biochem. J. **333**, 139–149

42 Hoffmann, R., Baillie, G. S., MacKenzie, S. J., Yarwood, S. J. and Houslay, M. D. (1999) The MAP kinase ERK2 inhibits the cyclic AMP-specific phosphodiesterase HSPDE4D3 by phosphorylating it at $Ser^{579}$. EMBO J. **18**, 893–903

43 Hill, E. V., Sheppard, C. L., Cheung, Y. F., Gall, I., Krause, E. and Houslay, M. D. (2006) Oxidative stress employs phosphatidyl inositol 3-kinase and ERK signalling pathways to activate cAMP phosphodiesterase-4D3 (PDE4D3) through multi-site phosphorylation at $Ser^{239}$ and $Ser^{579}$. Cell. Signalling **18**, 2056–2069

Received 20 July 2007/17 August 2007; accepted 30 August 2007
Published as BJ Immediate Publication 30 August 2007, doi:10.1042/BJ20070970

44 Perry, S. J., Baillie, G. S., Kohout, T. A., McPhee, I., Magiera, M. M., Ang, K. L., Miller, W. E., McLean, A. J., Conti, M., Houslay, M. D. and Lefkowitz, R. J. (2002) Targeting of cyclic AMP degradation to $\beta_2$-adrenergic receptors by $\beta$-arrestins. Science **298**, 834–836

45 Stefan, E., Wiesner, B., Baillie, G. S., Mollajew, R., Henn, V., Lorenz, D., Furkert, J., Santamaria, K., Nedvetsky, P., Hundsrucker, C. et al. (2007) Compartmentalization of cAMP-dependent signaling by phosphodiesterase-4D is involved in the regulation of vasopressin-mediated water reabsorption in renal principal cells. J. Am. Soc. Nephrol. **18**, 199–212